The Role of Intermolecular Hydrogen Bond on Dielectric Properties in Hydrogen-Bonded Material 5-Bromo-9-hydroxyphenalenone: Theoretical Investigation[†]

Hiroki Otaki[*] and Koji Ando

Dielectric properties of the hydrogen-bonded material, 5-bromo-9-hydroxyphenalenone ($C_{13}H_7O_2Br$; BrHPLN), are investigated theoretically by means of electronic structure calculations and Monte Carlo simulations. The density functional calculations of BrHPLN crystals have revealed that the polarization per one molecule can be about 1.7 times larger than that of the isolated monomer. It is also found that there exists significant electron density (0.01 e bohr^{-3}) in an intermolecular $C-H\cdots O$ region, which, together with the interatomic distances of 2.39 Å for $H\cdots O$ and 3.34 Å for $C\cdots O$, suggests the existence of intermolecular weak hydrogen bonding that may enhance the molecular polarization. The induced polarization effects in various intermolecular configurations are evaluated with the Fragment Molecular Orbital method. In addition to the π-π stacking interactions, two types of "in plane" intermolecular weak hydrogen-bonding configurations are found to affect the molecular dipole moment most significantly. These effects are efficiently included in a Monte Carlo simulation method in terms of "dipole corrections" as functions of both the intermolecular arrangements and the intramolecular proton configurations. The application to the dielectric phase transition of BrHPLN crystal shows that the dipole corrections almost double the transition temperature, toward better agreement with experiments, and qualitatively affect the temperature dependence of the dielectric constant. Discussions are given to support that the results will remain adequate and consistent even after explicit inclusion of the quantum tunneling effects.

1 Introduction

Ferroelectricity and antiferroelectricity have been very important topics in condensed matter physics. Since the first report of a ferroelectric phenomenon in an investigation of Rochelle salt in 1920,[1,2] a great number of ferroelectric and antiferroelectric materials have been discovered and widely used for industrial applications such as a ferroelectric random access memory (FeRAM) and a thermistor. Recently, great progress has been made in the materials design of organic ferroelectrics in the field of organic electronics.[3,4]

In the fundamental scientific interest, meanwhile, ferroelectrics have attracted much interest. One of the best known ferroelectric materials is potassium dihydrogen phosphate KH_2PO_4 (KDP).[5] In the KDP crystal, there exists an $O-H\cdots O$ hydrogen-bond network. Owing to the dimension and origin of the network, KDP is called a three-dimensional hydrogen-bonded system. A number of crystals isomorphous with KDP and other zero-, one-, two-, and three-dimensional hydrogen-bonded systems have been found to exhibit phase transitions.[6–8]

Most of the hydrogen-bonded systems exhibit large isotope effect, *i.e.*, the change of phase transition temperature induced by substitution of deuterium for hydrogen. For example, the transition temperature is almost doubled in the case of KDP and its family. The isotope effect has been investigated experimentally and theoretically for a long time.[9–11]

5-R-9-hydroxyphenalenone (R = Br, I or methyl group), belongs to hydrogen-bonded dielectrics. This group of materials is known as the zero-dimensional hydrogen-bonded system and synthesized artificially to study the isotope effect. As mentioned in Ref. 12, 5-R-9-hydroxyphenalenone seems to have only intramolecular hydrogen bonding and the hydrogen-bond length ($O\cdots O$ distance) is not affected much by the deuterium substitution. Therefore, these materials have been considered as ideal materials to investigate the effect of the deuteration separately from the Ubbelohde effect.[9,13]

Dielectric, calorimetric, spectroscopic and structural studies revealed that 5-bromo-9-hydroxyphenalenone ($C_{13}H_7O_2Br$; BrHPLN) and 5-methyl-9-hydroxyphenalenone ($C_{14}H_{10}O_2$; MeHPLN) exhibit the quite different behavior: the only BrHPLN shows a large isotope effect, although BrHPLN and MeHPLN have almost the same molecular and crystal structure in the high temperature range.[12,14–27] Both the H and D compounds of MeHPLN undergo the paraelectric-antiferroelectric phase transition around 42 K. In contrast, the H compound of BrHPLN (h-BrHPLN) exhibits no phase transition down to 3 K, while the D compound (d-BrHPLN) shows two phase transitions corresponding to the normal-incommensurate phase tran-

0 *Department of Chemistry, Graduate School of Science, Kyoto University, Sakyo-ku, Kyoto 606-8502, Japan. E-mail: hirotaki@kuchem.kyoto-u.ac.jp; Fax: +81-75-753-4018; Tel: +81-75-753-4022*

0 † Electronic supplementary information (ESI) available: Schematic structures and positions of BrHPLN trimers used for FMO calculations; additional NPA charges data.

sition at ~ 37 K and the incommensurate-commensurate one at ~ 20 K.[14,18,28] The d-BrHPLN crystal is also considered to be antiferroelectric in the low temperature region.

Kiyanagi *et al.* attributed the antiferroelectric property to the *local electronic dipole moment* in the hydrogen-bond region, which arises from the separation between the peaks of electron and nuclear density distributions resulted from the X-ray and neutron diffraction experiments.[22,25,27] Their analysis shows that the *local electronic dipole moment* pointing from the enolic oxygen to the carbonic oxygen within the molecule has the magnitude $0.9 \sim 2.2$ D, and the resulting dipole-dipole interaction energy corresponds well with the phase transition temperature. However, our calculation (see Fig. 1) shows that the transverse component of the molecular dipole moment points the opposite direction and its magnitude is much smaller compared to their *local electronic dipole moment*. This indicates that we need more careful analysis taking better account of the molecular aspects.
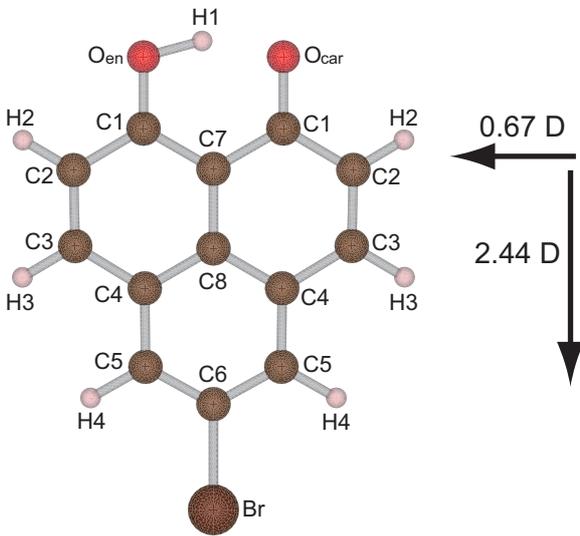

Fig. 1 Schematic structure of the enol-form tautomerization of BrHPLN and the atomic labels. The two oxygen atoms, O_{en} and O_{car}, denote an enolic oxygen and a carbonic oxygen, respectively. The thick arrows indicate the transverse and longitudinal components of the dipole moment, which are calculated with the HF/3-21G(d,p) level. For the molecular and crystallographic drawings in this paper, the software VESTA was used.[29]

In a previous theoretical study, a simple three-site model was proposed to describe the isotope effect of the zero-dimensional hydrogen-bonded ferroelectrics and antiferroelectrics.[30,31] More recently, quantum chemical calculations were performed for several neighboring dimers of BrHPLN and 5-iodo-9-hydroxyphenalenone (IHPLN).[32,33] The tunneling parameter and interaction parameter of the transverse Ising model[10,34] were calculated and the ordered phase at the low

temperature limit was discussed on the basis of the mean field approximation. Although these works have provided intriguing clues under their approximations, in our view, more extensive analysis will be needed for elucidation of the dielectric properties arising from the intricate intermolecular interactions in the crystal. For instance, it has been shown in the case of another π-conjugated hydrogen-bonded organic ferroelectric, phenazine-chloranil acid (Phz-H_2ca), that intermolecular hydrogen bonds of $O - H \cdots N$ type significantly enhance the electronic polarization.[35,36] In BrHPLN and its families, on the other hand, there exist analogous $C - H \cdots O$ type intermolecular arrangements. This type of bonding is known as the weak hydrogen bond, whose existence is recognized in many chemical and biological systems,[37,38] but their roles are in most cases yet unclear.

In this paper, from this point of view, we focus on the effect of the intermolecular hydrogen bond on the dielectric properties of BrHPLN. To our knowledge, the realistic molecular calculations beyond the dimer interactions and the Monte Carlo simulations with long-range interactions taking account of the induced polarization effects have been done for the first time. We use density functional theory (DFT) with plane-wave basis sets[39] and the Fragment Molecular Orbital (FMO) method[40] in order to evaluate the effect of the intermolecular hydrogen bond. Then we shall show that the effect of the intermolecular hydrogen bond is significant to the dielectric properties of BrHPLN. In addition, we performed Monte Carlo (MC) simulations in order to determine the microscopic ordering in the antiferroelectric phase in the low temperature. We also propose a Monte Carlo method with the correction of the dipole moment, reflecting the results of the FMO calculation. The quantitative discussion of the phase transition temperature is given by comparing the results of the MC simulations with and without the correction.

The paper is organized as follows. In Sec. 2, we give brief explanation of computational methods. Sec. 3 is devoted to results and discussions. The paper ends with some concluding remarks in Sec. 4.

2 Methods

2.1 Several Settings

We begin with some settings for the calculation. The BrHPLN molecule has two energetically equivalent enol-form tautomers and these two states are equilibrium states in a symmetric double-well potential. It is considered that the tunneling transfer of a proton takes part in the tautomerization between the equilibrium states. For sake of simplicity, however, we do not explicitly consider the quantum tunneling effect but only briefly discuss its possible consequences in Sec. 3.3. In addition, we take no account of the decrease of the crystal sym-
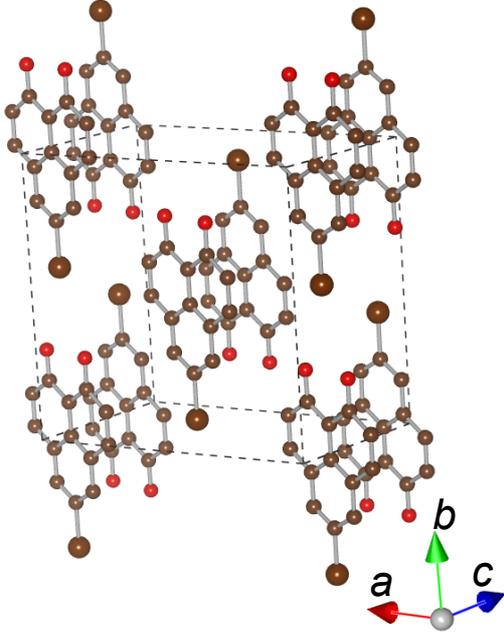
Fig. 2 Schematic structure of BrHPLN crystal (hydrogen atoms are not shown).

metry from $C2/c$ to $P2_1/c$, which occurs with the paraelectric-antiferroelectric phase transition, but with minor (and continuous) structural change, *ca.* 3% of volume change and a few degrees of angular distortion.[18,25] The deuteration does not affect the molecular structure of BrHPLN in the room temperature. Thus, through the paper we use the molecular structural data of h-BrHPLN on the neutron diffraction data at 10 K which is shown in Ref. 27. In Fig. 1 and Fig. 2, we show the schematic molecular and crystal structure, respectively. The crystal system of h-BrHPLN at 10 K is monoclinic and the space group is $C2/c$ (#15; $Z = 4$). The lattice parameters are set to be $a = 11.959$ Å, $b = 11.685$ Å, $c = 7.010$ Å and $\beta = 97.54°$. We here refer the point 0.25 Å distant from C8 toward C7 as a molecular center. (Note that the molecular center is *not* the center of the mass.) In the direction of the c-axis, the molecules are arranged such that the molecular centers are aligned in a straight line. In this paper, we assume that these structural parameters are kept through the whole temperature range. In addition, we set up a Cartesian coordinate system so that x- and y-axis coincide with the crystallographic a- and b-axis, respectively.

In Fig. 1, the dipole moment of BrHPLN is also shown. Since all of the atoms in the BrHPLN molecule are almost coplanar, the molecular dipole moment $\mathbf{p} = (p_x, p_y, p_z)$ lies in the molecular plane. We thus define the components of the dipole moment parallel and perpendicular to the b-axis as the longitudinal ($p_\parallel = p_y$) and transverse ($p_\perp = \sqrt{p_x^2 + p_z^2}$) dipole

moments, respectively. These two parameters are often used in the following discussions. The transition of the hydrogen atom in the intramolecular hydrogen bond (H1 in Fig. 1) from one equilibrium state to the other inverts the transverse dipole moment. In the following, we refer to the configuration of the hydrogen atom H1 as "H-configuration", and use the expression L (R) when the hydrogen atom H1 is bonding to the left (right) oxygen atom viewed in the direction of the c-axis.

2.2 Density Functional Calculation with Plane-Wave Basis Set

As a first step, we investigate the effect of intermolecular bonding for the electric polarization of BrHPLN by calculating spontaneous polarization with the Berry phase method.[41,42] To facilitate the calculation of the dielectric polarization per molecule by the Berry phase method, all the H1 atoms are placed (virtually) on the same side such that all the transverse components of molecular dipoles align in the same direction. We performed *ab-initio* plane-wave density functional calculation with generalized gradient approximation (GGA) using the PWSCF package in QUANTUM ESPRESSO.[43] We use the Perdew-Burke-Ernzerhof (PBE) exchange-correlation functional and ultrasoft pseudopotentials with the kinetic energy cutoff of 30 Ry for wave functions and 300 Ry for charge density. The **k**-space integration is achieved with a finite **k**-point mesh for monoclinic reciprocal unit lattice vectors ($\mathbf{a}^*$, $\mathbf{b}^*$, $\mathbf{c}^*$). We have used the (4, 1, 2) **k**-point mesh for self-consistent-field (SCF) calculations. After the SCF calculations, the calculation of the spontaneous polarization is carried out with the (10, 1, 2) **k**-point mesh. In order to check the convergence of the spontaneous polarization, the calculation is performed with different mesh sizes: the (10, 2, 4) **k**-point mesh for the SCF calculations and the (20, 2, 4) **k**-point mesh for the calculation of the spontaneous polarization.

2.3 FMO Calculation

By the Berry phase density functional calculation in the previous section, we can see that the polarization of the molecule is affected by its surrounding molecules (See Sec. 3.1). The plane-wave density functional approach, however, cannot be applied to evaluate the polarization per one molecule of antiferroelectric systems in which the net polarization vanishes. As the next step, in order to specify what positional relations of the molecules strongly affect each other and how different is the effect by each H-configuration of the environmental molecules, we performed quantum mechanical calculations with the FMO method.[40] In the FMO-2 scheme, a whole molecular system is divided into small fragments and *ab-initio* calculations are carried out for each fragment monomer and fragment dimer. In the FMO method, dipole moments for each fragment are also cal-

Table 1 List of the trimers calculated with the FMO method. Relative positions for the molecular centers of the molecules are given which form the trimers with a reference (0, 0, 0) molecule. The H1 atom of the reference molecule is arranged on the upper side in the longitudinal direction ($+b$). The positions X, Y and Z are written in units of the lattice parameters a, b and c, respectively. (The double sign applies in the same order.) The schematic structures of these trimers are given in Figs. S1-S14 in the ESI.† In the Cartesian coordinates defined in Sec. 2.1, the positions are expressed as $x = Xa + Zc\cos\beta$, $y = Yb$, and $z = Zc\sin\beta$

Trimer	Position			Trimer	Position		
	X	Y	Z		X	Y	Z
A	±1.0	0.0	0.0	H	±0.5	-0.5	±0.5
B	0.0	±1.0	0.0	I	±0.5	0.5	±0.5
C	0.0	-1.0	±0.5	J	±0.5	-0.5	∓0.5
D	0.0	1.0	±0.5	K	±0.5	0.5	∓0.5
E	0.0	0.0	±1.0	L	0.0	0.0	±0.5
F	±0.5	-0.5	0.0	M	±1.0	0.0	±0.5
G	±0.5	0.5	0.0	N	±1.0	0.0	∓0.5

culated. Therefore, by regarding one molecule as one fragment, we can evaluate the difference of the dipole moment influenced by the surrounding molecules from that of an isolated BrHPLN molecule. We used the program GAMESS[44] for the FMO calculations.

Before the calculation we classified the neighboring molecules by their relative positions from one molecule by using the crystal structural data. Because of the crystal symmetry, there exist two molecules in the same positional relation. Therefore, we can construct a trimer with the two molecules and the reference molecule. We set up the 14 types of trimers listed in Table 1, which include all the nearest-neighbor molecules and next-nearest-neighbor molecules along the c-axis. The schematic structures of the trimers and their positions in the crystal are shown in Figs. S1-S14 in the ESI.† For each of the trimers, the calculation was done in all the cases of the H-configurations of two surrounding molecules (LL, LR, RL, and RR) with the H-configuration of the central molecule fixed to be L, It is sufficient to calculate with the H-configuration of the central molecule fixed to be one side, because of the crystal symmetry.

The calculation results are evaluated with the relative change of the dipole moment of the central molecule in each trimer $\mathbf{p}^{\mathrm{FMO}} = (p_x^{\mathrm{FMO}}, p_y^{\mathrm{FMO}}, p_z^{\mathrm{FMO}})$ from the dipole moment calculated with the isolated monomer $\mathbf{p}^{\mathrm{mon}} = (p_x^{\mathrm{mon}}, p_y^{\mathrm{mon}}, p_z^{\mathrm{mon}})$. It is obvious that $\mathbf{p}^{\mathrm{FMO}}$ depends on the H-configuration of the molecules. We introduce the sign parameter $s_i = \pm1$ with $i = 1, 2$ and 3, where the sign corresponds to the direction of the transverse dipole moment: -1 (H-configuration: L) and $+1$ (H-configuration: R). The subscript i labels the molecules of the trimers. The molecule 2 is the central one and the molecules 1 and 3 are its surrounding ones. Then, the relative change of

the dipole moment is defined as

$$\Delta p_\mu(s_1, s_2, s_3) = \left| \frac{p_\mu^{\mathrm{FMO}}(s_1, s_2, s_3)}{p_\mu^{\mathrm{mon}}} \right| - 1, \quad (1)$$

with $\mu = x, y$ and z. Moreover, we define the transverse/longitudinal dipole moments of the central molecule in each trimer and the isolated monomer as mentioned in Sec. 2.1, i.e., $p_\perp^{\mathrm{FMO}} = \sqrt{(p_x^{\mathrm{FMO}})^2 + (p_z^{\mathrm{FMO}})^2}$, $p_\parallel^{\mathrm{FMO}} = p_y^{\mathrm{FMO}}$, $p_\perp^{\mathrm{mon}} = \sqrt{(p_x^{\mathrm{mon}})^2 + (p_z^{\mathrm{mon}})^2}$, and $p_\parallel^{\mathrm{mon}} = p_y^{\mathrm{mon}}$. Then, the relative changes of the transverse and longitudinal dipole moment are also written as

$$\Delta p_\perp(s_1, s_2, s_3) = \left| \frac{p_\perp^{\mathrm{FMO}}(s_1, s_2, s_3)}{p_\perp^{\mathrm{mon}}} \right| - 1, \quad (2)$$

and

$$\Delta p_\parallel(s_1, s_2, s_3) = \left| \frac{p_\parallel^{\mathrm{FMO}}(s_1, s_2, s_3)}{p_\parallel^{\mathrm{mon}}} \right| - 1 = \Delta p_y(s_1, s_2, s_3), \quad (3)$$

respectively.

2.4 Monte Carlo Simulation with Dipole Moment Correction

The dielectric properties of the crystal system were investigated by performing Monte Carlo simulations. In this study, we do not take into account the proton tunneling process. This means that the properties of BrHPLN in the classical limit are investigated. In the MC simulation, we consider the dipolar system on the 3D lattice of BrHPLN. In the system, each molecular electric dipole is located at the center of the mass of the molecule (1.79 Å from C8 toward Br) and the dipoles interact with other dipoles through dipole-dipole interactions. Taking the H-configuration into account, we can assume that each dipole moment has discrete values.

We here define a unit cell for the MC simulation (MC unit cell). Figure 3 shows the MC unit cell. Since the molecular crystal of BrHPLN has face-centered molecules, the MC unit cell is set in a slightly different manner from the crystallographic unit cell. The MC unit cell consists of two unit cells along the a- and b- axis and one unit cell along the c-axis, which means that the MC unit cell is a $2a \times 2b \times c$ monoclinic lattice. Furthermore, we define N_a, N_b and N_c as the number of the MC unit cells along the a-, b- and c-axis, respectively. The total number of the molecules considered in the MC calculation N is written as $N = 16 N_a N_b N_c$.

In this work, we correct the dipole moment obtained from the calculation for the isolated monomer by using $\Delta p_\mu(s_1, s_2, s_3)$ in Eq. (1). For every site j, we compose the trimers in Table 1 so that site j is the central molecule for each of the trimers, and apply the relative changes obtained from the FMO calculation
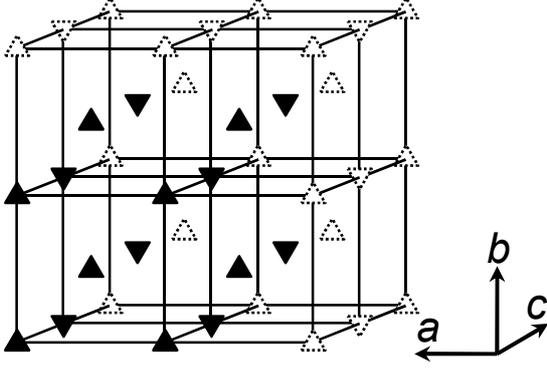
Fig. 3 Unit cell for Monte Carlo simulation (MC unit cell). Each triangle indicates a BrHPLN molecule and inverted triangle represents an inverted one. The molecular electric dipole is located at the center of the mass. The dotted triangles are not included in the MC unit cell but belong to the next ones.

according to the H-configurations of the trimers. Assuming that the relative changes can be linearized with all the trimers, we can write corrected dipole moment of site j as

$$p_{j\mu} = \left(1 + \sum_\alpha \Delta p_\mu(s_1^{\alpha j}, s_j, s_3^{\alpha j})\right) p_\mu^{\mathrm{mon}}, \quad (4)$$

with $\mu = x, y$ and z, where s_j and $s_i^{\alpha j}(i = 1, 3)$ denote the H-configurations of the site j and the sites which compose trimer α with site j, respectively. The summation of α is taken over all the trimers considered. Therefore, using $\mathbf{p}_j = (p_{jx}, p_{jy}, p_{jz})$, the Hamiltonian of the system is written as

$$\mathscr{H} = \frac{1}{4\pi\varepsilon_0} \sum_{j<k} \frac{1}{r_{jk}^3} \left[\mathbf{p}_j \cdot \mathbf{p}_k - \frac{3(\mathbf{p}_j \cdot \mathbf{r}_{jk})(\mathbf{p}_k \cdot \mathbf{r}_{jk})}{r_{jk}^2}\right], \quad (5)$$

with $r_{jk} = |\mathbf{r}_{jk}|$, where $\mathbf{r}_{jk}$ is the position vector from site j to k and ε_0 is the vacuum permittivity. In the MC simulation, s_j can be flipped in every Monte Carlo trial. The dipole moments can be corrected according to Eq. (4) in every MC step, where 1 MC step consists of a series of trials throughout the lattice. From now on, we will refer to this procedure as "dipole correction" here.

We have used the replica exchange Monte Carlo method[45] with periodic boundary condition. For updating of each replica, we have adopted the Metropolis algorithm. The number of the replicas for the exchange Monte Carlo method is 80 between 5 K and 130 K, distributed at regular intervals. The temperature of each replica is fixed throughout simulations. Initial configurations of the replicas were taken randomly and all replicas were thermalized without being exchanged. After the thermalization, one exchange trial between replicas was made every 5 MC steps (one replica-exchange step) and data were

collected at every replica-exchange step. We take 20000 MC steps for the thermalization and 300000 MC steps for the measurement. Investigated system sizes are $(N_a, N_b, N_c) = (3, 3, 9)$, $(4, 4, 12)$ and $(5, 5, 15)$, corresponding to $N = 1296, 3072$ and 6000 dipoles, respectively. The cutoff radius r_c for the dipole-dipole interaction is set to be 20 Å. In the case without the dipole correction, the maximum value of coupling parameters with the dipole outside this radius is 0.49 K, which is small enough compared with the critical temperature evaluated by our calculation (See Sec. 3.3). Using the above conditions, we performed the MC simulation with or without the dipole correction.

3 Results and Discussion

3.1 Spontaneous Polarization, Charge Density and NPA Charges

We consider three types of crystal structures shown in Fig. 4, which differ in density. Crystal (a) is the original structure of BrHPLN. Crystal (b) has the structure in which face-centered molecules are removed from crystal (a). In crystal (c), the face-centered molecules are also removed and the distance between neighboring molecules in the same stack is three times longer than that of crystal (b).

The longitudinal polarization is canceled because of the crystal symmetry. The calculated transverse polarizations per one molecule are (a) 1.04 D, (b) 0.45 D and (c) 0.60 D. The results have been checked to converge within 0.01 D for the use of different **k**-point mesh sizes. It is obvious that the BrHPLN molecule is strongly affected by its surrounding molecules. Comparison between (a) and (b) shows that the interaction between the neighboring molecules in the same layer increase the polarization. However, the closer the distance with neighboring molecules in the same stack is, the smaller the polarization becomes. This is considered to be the effect of the π-π stacking interaction, which appears in trimer L in Table 1 and Fig. S12 in the ESI.† It should be noted that each molecule in crystal (c) is approximately isolated and the result is the same order as the calculated result of the monomer (See Fig. 1).

We also calculated the electron charge density of BrHPLN. The calculated charge density contour map is shown in Fig. 5. In this plot, the charge density is viewed normal to $(\overline{2}03)$ plane and the positional relation of the molecules is the same as that of trimer I in Table 1 (See also Fig. S9 in the ESI†). As can be seen, the charge density at the intermolecular region amounts to 0.01 e bohr^{-3}. It has been reported that this amount of charge density is significant in intermolecular regions in the case of other organic molecular ferroelectric systems: this charge density mediates the intermolecular covalency and strongly enhances the electronic polarization.[35,36] In BrHPLN, a hydrogen atom (H2) of one molecule is close to an oxygen atom of an-
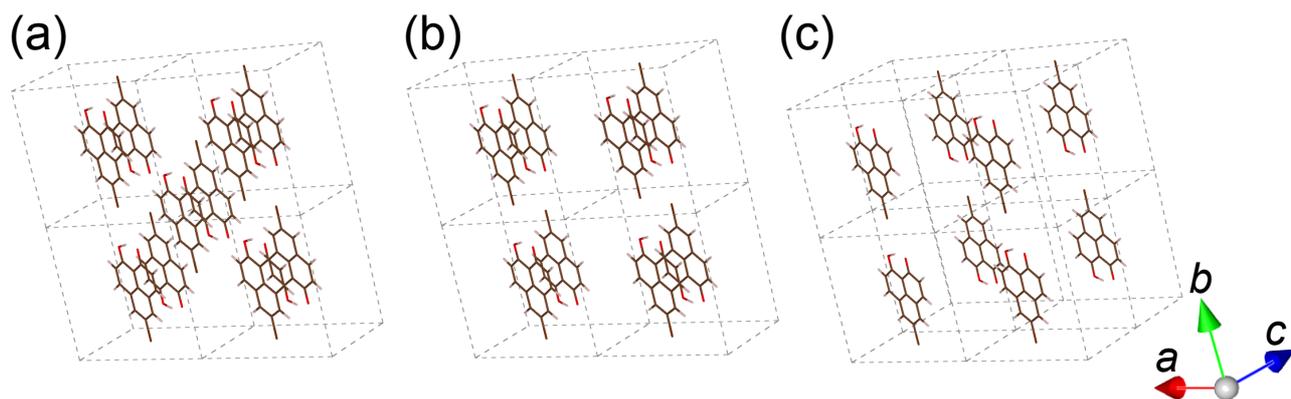
Fig. 4 Three types of crystal structures used for plane-wave density functional calculation. (a) Original crystal structure. (b) Structure in which face-centered molecules are removed from the original structure. (c) Structure in which the distance between neighboring molecules in the same stack is three times longer than that of (b).
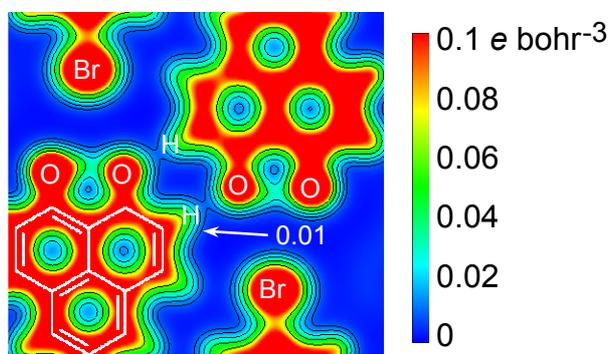

Fig. 5 Charge density of BrHPLN viewed normal to $(\bar{2}03)$ plane. Contours are drawn on a logarithmic scale from 0.01 e bohr^{-3} to 0.1 e bohr^{-3}. The color scale is linear from blue to red as charge density increases.
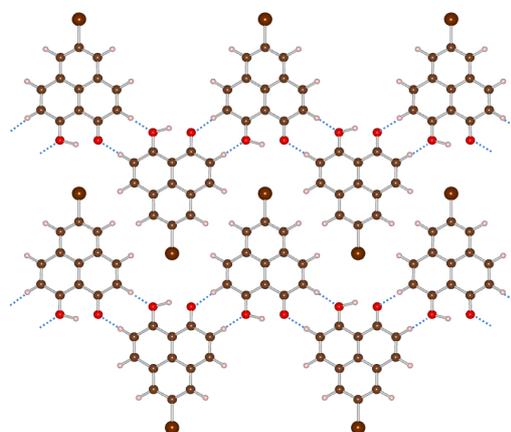
Fig. 6 Schematic showing the one-dimensional intermolecular hydrogen-bond chains in BrHPLN (viewed along the *c*-axis).

other molecule. From the crystallographic data, we obtain the lengths of H2$\cdots$O and C2$\cdots$O as 2.39 Å and 3.34 Å, respectively. This type of configuration, C$-$H$\cdots$O, is well known as the weak hydrogen bond and the lengths mentioned above satisfy the criterion of the weak hydrogen bond.[38] Therefore, the results suggest that there exist one-dimensional chains of the intermolecular weak hydrogen bonds and the chains make great contribution to the dielectric properties in the BrHPLN crystal. In Fig. 6, we show the schematic view of the intermolecular bonding chains.

The role of the intermolecular weak hydrogen bond is further examined by the natural population analysis (NPA)[46] from the FMO calculations. The NPA is recognized as more robust population analysis against the variation of the size of the basis set. We employed NPA for the isolated monomer and trimer I in Table 1 (See also Fig. S9 in the ESI†), assuming that all the

molecules are in the same H-configuration. In Fig. 7, we show the schematic structure of trimer I and labels of atoms used for NPA. The results are shown in Table 2. In the trimer case, it is seen that the charges of the oxygen atoms and those of the hydrogen atoms close to the oxygen atoms of another molecule become more negative and positive than in the case of the isolated monomer, respectively. On the other hand, there is little change in the charge of H1 and C2 atoms. This suggests that the oxygen atoms attract the electrons of the hydrogen atoms of the neighboring molecules, leading to the increase of the intermolecular covalency.

Another type of C$-$H$\cdots$O configurations is also seen in trimer F, which satisfy the criterion of the weak hydrogen bond shown in Ref. 38. Figure 8 and Table 3 show the schematic structure and the NPA charges of trimer F, respec-

Table 2 NPA charges for the isolated monomer and the central molecule of trimer I. The atomic charges of H2 and C2 close to the enolic oxygen (H2($\cdots$O$_{en}$) and C2($\cdots$O$_{en}$)) and the carbonic oxygen (H2($\cdots$O$_{car}$) and C2($\cdots$O$_{car}$)) of another molecule are shown separately. For the labels of atoms, see Fig. 7

	HF/3-21G(d,p)		HF/6-31G(d,p)	
Atom	Isolated	Central	Isolated	Central
O$_{car}$	−0.699	−0.725	−0.777	−0.803
H2($\cdots$O$_{car}$)	0.249	0.266	0.254	0.275
C2($\cdots$O$_{car}$)	−0.334	−0.333	−0.327	−0.324
O$_{en}$	−0.723	−0.736	−0.770	−0.784
H2($\cdots$O$_{en}$)	0.249	0.260	0.254	0.267
C2($\cdots$O$_{en}$)	−0.323	−0.328	−0.317	−0.320
H1	0.533	0.533	0.584	0.582

Table 3 Same as Table 2, but for trimer F. The charges of H1 of the surrounding molecules are omitted because there are not significant differences (less than 0.001)

	HF/3-21G(d,p)		HF/6-31G(d,p)	
Atom	Isolated	Central	Isolated	Central
O$_{car}$	−0.699	−0.712	−0.777	−0.793
H4($\cdots$O$_{car}$)	0.253	0.259	0.262	0.267
C5($\cdots$O$_{car}$)	−0.144	−0.149	−0.154	−0.158
H3($\cdots$O$_{car}$)	0.236	0.246	0.242	0.254
C3($\cdots$O$_{car}$)	−0.109	−0.104	−0.112	−0.105
O$_{en}$	−0.723	−0.732	−0.770	−0.781
H4($\cdots$O$_{en}$)	0.252	0.255	0.260	0.262
C5($\cdots$O$_{en}$)	−0.143	−0.149	−0.152	−0.158
H3($\cdots$O$_{en}$)	0.238	0.244	0.244	0.252
C3($\cdots$O$_{en}$)	−0.095	−0.092	−0.099	−0.094
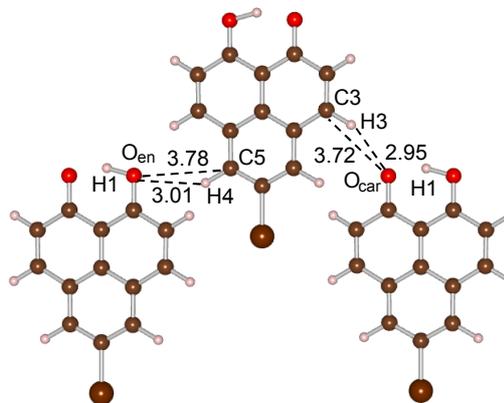
Fig. 8 Same as Fig. 7, but for trimer F.

Fig. 7 Schematic structure of trimer I. Labels for atoms are also shown. The values in the figure denote the distances between atoms (in Å).

tively. As can be seen, there exist two types of the configurations: C3 − H3$\cdots$O and C5 − H4$\cdots$O. The interatomic distances in these configurations are longer than those of trimer I. Moreover, the differences of the NPA charges between the isolated molecule and the central molecule of trimer F are smaller than those of trimer I. Therefore, it is considered that the effect of the intermolecular bonding is smaller than that of trimer I. In trimer F, the intermolecular charge density is about 0.003 e bohr^{-3}.

In trimer F, there is a large difference in the NPA charge of the Br atom (See Table S1 and Fig. S15 in the ESI†). As is seen in Table S1 in the ESI,† some hydrogen and carbon atoms of the surrounding molecules are affected by the Br atom. The Br atom may thus contribute to the intermolecular bonding. Nonetheless, we shall reserve this issue for future investigations to compare with the other substituents such as MeHPLN and IHPLN.

3.2 Dependence on positional relations and H-configurations

In the previous section, we show that the intermolecular bonding makes the significant change in the dipole moment. We next discuss the change of the dipole moment induced by the surrounding molecules. Figure 9 shows the results obtained from the FMO calculation. In Fig. 9, the horizontal axis is the labels of the trimers defined in Table 1 and the vertical axis is $\Delta p_\perp(s_1, s_2, s_3)$ and $\Delta p_\parallel(s_1, s_2, s_3)$ defined by Eqs. (2) and (3), respectively. The transverse component is mainly affected by three types of trimers, F, I, and L, which make more than 20% of differences from the dipole moment of the isolated monomer. This result is consistent with the result of the previous section. Furthermore, in these trimers, the change of the dipole moment strongly depends on the H-configurations of the surrounding molecules. On the other hand, the longitudinal component is also affected by the environmental molecules. This, however, depends on rather the type of the trimers than the H-configurations. This result is reasonable because this direction is perpendicular to the reversible component with the proton transfer. We consider that the effect of this direction is averaged out in the crystal.

3.3 Monte Carlo simulation

From the results in the previous section, we could impose the condition on the MC simulation as follows. First, only the relative changes of trimers F, I and L are used for the dipole correction of the transverse component. Second, the relative changes of the longitudinal component are not taken into account. Henceforth, we show the results of the MC simulation in which the result of the HF/3-21G(d,p) level is used for the value of p_μ^{mon} in Eq. (4).

The paraelectric-antiferroelectric phase transition was found by the measurement of the dielectric constant along the *a*-axis.[12,14] We thus calculate the *x*-component of the polarization per unit volume P_x, which is defined as

$$P_x = \frac{4}{V} \sum_j p_{jx}, \qquad (6)$$

where V is the volume of the system calculated. The fact is well known that the order parameter (*e.g.*, P_x) still remains in the order of $1/\sqrt{N}$ even at infinite temperature.[47] We thus employ finite size scaling for our simulation results. Figure 10 shows the scaled plot of the absolute value $|P_x|$ for several system sizes with or without the dipole correction. It is seen that the curves for the different system sizes are scaled well by $\sqrt{N}$. In the high temperature range, which corresponds to a paraelectric phase, the polarization of the system is enhanced because of the dipole correction.

In both cases, we can see that the polarization tends to zero as temperature decreases. For more detailed description of the low
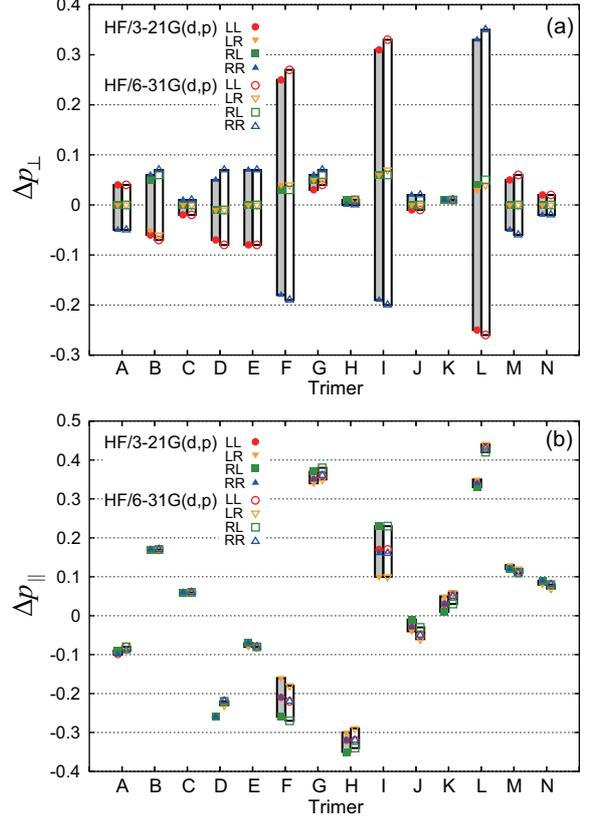

Fig. 9 Relative change of the (a) transverse and (b) longitudinal dipole moment. In each type of the trimers, four values corresponding to the combination of the H-configurations of the surrounding molecules (LL, LR, RL, and RR) are plotted for the case of the HF/3-21G(d,p) level (closed symbol) and HF/6-31G(d,p) level (open symbol). The bars represent the range between the maximum and minimum for each type of the trimers.
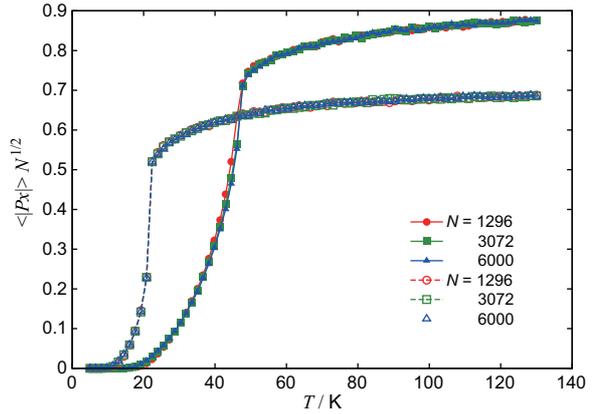

Fig. 10 Scaled plot of *x*-component of polarization $|P_x|$. Data for different system sizes (*N*) with (closed symbol) or without (open symbol) the dipole correction are plotted as functions of temperature.

8
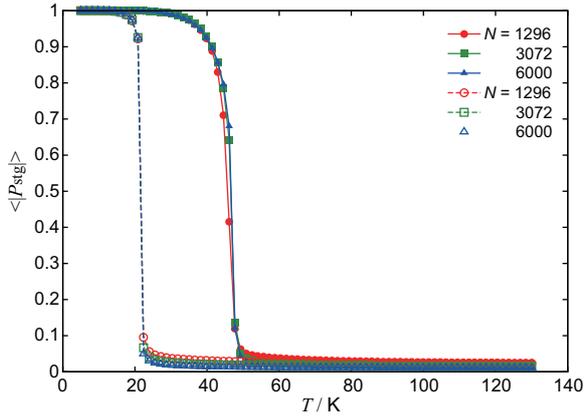
Fig. 11 Absolute value of the staggered polarization $|P_{stg}|$. Data for different system sizes (N) with (closed symbol) or without (open symbol) the dipole correction are plotted as functions of temperature.


Fig. 12 Schematic diagram of the antiferroelectric state obtained from the MC simulation. In this ordered state, the corrected transverse dipole moment is evaluated as 0.98 D.

temperature phase, let us introduce the order parameter P_{stg}, which is called the staggered polarization. If we write the position of the site j as (a_j, b_j, c_j) with the same manner as Table 1, a_j, b_j and c_j can take integer or half-integer values. Using these parameters, we define P_{stg} as

$$P_{stg} = \frac{1}{N} \sum_{j=1}^{N} (-1)^{2(a_j+c_j)} s_j. \tag{7}$$

The parameter P_{stg} is equal to 1 or -1 in the case where all of the transverse dipole moments of the neighboring molecules along the c-axis and $(\pm 1/2, \pm 1/2, 0)$ directions are antiparallel. In Fig. 11, we show the temperature dependence of the absolute value of the staggered polarization in our system. As can be seen, $|P_{stg}|$ changes drastically with temperature and $|P_{stg}|$ is nearly equal to 1 in the low temperature range. From these results, we conclude that a phase transition from a paraelectric phase to an antiferroelectric phase occurs in BrHPLN; this result corresponds to the experimental results. By the definition of P_{stg}, polarization ordering in the antiferroelectric phase can be drawn as shown in Fig. 12.

As is seen in Fig. 10 and Fig. 11, the critical temperature of the system T_c with the dipole correction becomes larger than T_c without the dipole correction. In order to compare with the experimental data, we define the critical temperature T_c in the same manner in Ref. 12 and Ref. 14 , *i.e.*, the peak position of the dielectric constant ε, although the Binder parameter is usually used in Monte Carlo study.[47] In Fig. 13, we show the temperature dependence of the static dielectric constant. The calculated static dielectric constant is comparable with that obtained from the experiments,[12,14] although the experimental result is the dynamic dielectric constant measured at a frequency of 10 kHz. We refer to the critical temperature T_c as ~ 24 K without the dipole correction and ~ 50 K with the dipole cor-

rection. The dipole correction, which is introduced in order to include the effect of the intermolecular weak hydrogen bonding, brings about an amplification of the molecular dipole moment and leads to increasing the critical temperature.
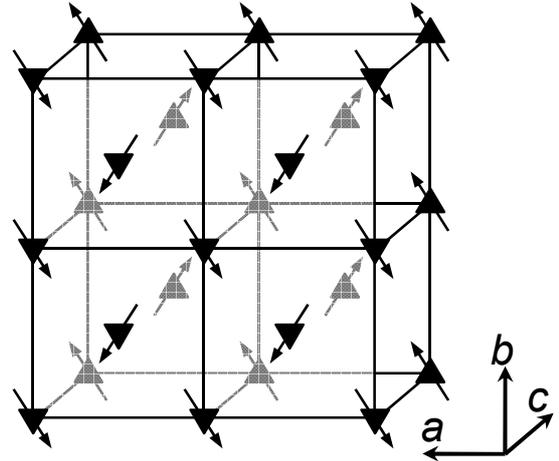
The critical temperature with the dipole correction is still higher than that of d-BrHPLN from experiments (37 K). There are, however, two reasons to support the present computational results. First, inclusion of the quantum tunneling effect is expected to improve the correspondence with the experiment. As is shown below, the tunneling effect is represented by the tunneling frequency Ω in the transverse Ising model[34] and Ω is estimated to be about 10 K for d-BrHPLN. Therefore, the inclusion of this tunneling frequency will reduce the T_c toward better agreement with the experiment (See below for the detail). Second, the dipole moment of the BrHPLN monomer depends on basis sets. In Table 4, we show dipole moments calculated by using several basis sets. We can see that the electron correlation and intramolecular polarization strongly affect the dipole moment. In particular, the inclusion of the electron correlation leads to a notable decrease of the transverse dipole moment. We may therefore roughly estimate that if the electron correlation effect were included, the computed T_c will be reduced by the factor of $(2.278/2.529)^2 \sim 0.8$, *i.e.*, the square of the ratio between the net dipole moments from HF/3-21G(d,p) and MP2/LANL2DZ(d,p), as implied from Eq. (5). It would be intriguing to explore the electron correlation effect more quantitatively, which we plan to report in future in conjunction with its influence on the potential barrier height along the proton displacements.

Finally, we mention the correspondence with the transverse Ising model,[10,48] which is often used in the study of hydrogen-bonded ferroelectrics. The Hamiltonian of the transverse Ising

9
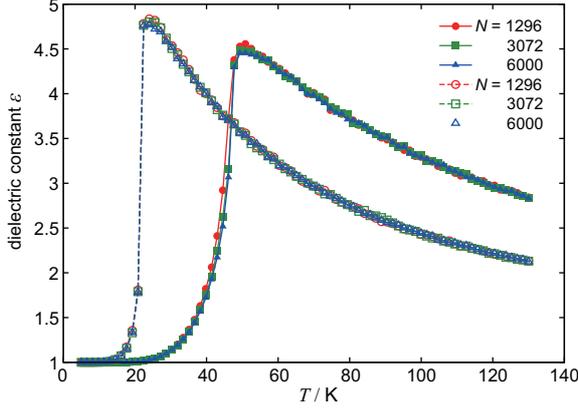
Fig. 13 Dielectric constant $\varepsilon = 1 + \chi$, where the electric susceptibility χ is calculated as the fluctuation of P_x. Data for different system sizes (N) with (closed symbol) or without (open symbol) the dipole correction are plotted as functions of temperature.

Table 4 Dipole moment of the BrHPLN monomer calculated with several computational levels

Computational level	Dipole moment / D		
	$\left\|p_\perp^{\mathrm{mon}}\right\|$	$\left\|p_\parallel^{\mathrm{mon}}\right\|$	$\left\|p^{\mathrm{mon}}\right\|$
HF/3-21G	0.558	3.614	3.656
HF/3-21G(d,p)	0.675	2.438	2.529
HF/6-31G	0.643	3.933	3.985
HF/6-31G(d,p)	0.742	2.928	3.020
MP2/LANL2DZ(d,p)	0.466	2.230	2.278
MP2/cc-pVDZ(-PP)[a]	0.415	1.649	1.700

[a] The cc-pVDZ basis set was used for H, C and O, and the cc-pVDZ-PP basis was used for Br.

model is written as

$$\mathcal{H} = -\Omega \sum_i \sigma_i^x - \sum_{i,j} J_{ij} \sigma_i^z \sigma_j^z, \tag{8}$$

where $\sigma_i^\alpha (\alpha = x, z)$ are Pauli matrices, J_{ij} is the coupling parameter between sites i and j, and Ω is the tunneling frequency. The mean field theory of the transverse Ising model tells us that the result depends on the ratio $\Omega/|J|$, where J is the molecular field parameter $\sum_j J_{ij}$.[34,49] For $\Omega/|J| < 1$ the ordered phase appears, while it disappears for $\Omega/|J| > 1$. In our dipolar system, the coupling parameter J_{ij} is calculated using the following relation:

$$J_{ij} = -\frac{1}{4} \left(E_{ij}^{(\mathrm{LL})} + E_{ij}^{(\mathrm{RR})} - E_{ij}^{(\mathrm{LR})} - E_{ij}^{(\mathrm{RL})} \right), \tag{9}$$

where $E_{ij}^{(h_i h_j)}$ is the dipole-dipole interaction energy between the two sites in the case where the H-configurations of site i and j are h_i and h_j, respectively. By the definition, when J_{ij}

is positive (negative), the interaction is ferroelectric (antiferroelectric). By using Eq. (9), the molecular field parameter J is evaluated to be $J = -20$ K with $r_c = 20$ Å in the case without the dipole correction. This value is consistent with $T_c \sim 24$ K obtained from the MC simulation. In the case with the dipole correction, on the other hand, it is difficult to determine J_{ij} because of the increase/decrease of the dipole moment according to the H-configurations of the surrounding molecules. However, from our result of the MC simulation, we can estimate J as about -50 K in the system.

Although the experimental value of the tunneling frequency for d-BrHPLN, Ω_D, is unavailable, we estimate it from other available data in the following way. First, the experimental tunneling frequency of h-BrHPLN is known to be $\Omega_H = 60$ K.[17] We then refer to the related compound, 9-hydroxyphenalenone, isolated in solid neon, for which the tunneling frequencies of both the H and D compounds have been measured spectroscopically as $\Omega_H = 50$ K and $\Omega_D = 8.6$ K, respectively.[50] Assuming that the ratio Ω_H/Ω_D carries over for the BrHPLN compounds, we can estimate the tunneling frequency of d-BrHPLN as $\Omega_D = 10$ K. Therefore, if we extend our method to treat the quantum tunneling effect just like the transverse Ising model, we can obtain some results which are consistent with the experimental data.

In the mean field theory, the transition temperature T_c is represented as

$$\frac{1}{|J|} = \frac{1}{\Omega} \tanh\left(\frac{\Omega}{k_B T_c} \right), \tag{10}$$

where k_B is the Boltzmann constant.[11,51] Substituting the value of J and Ω_D into Eq. (10), we estimate that the transition temperatures are corrected to 49 K from 50 K (with the dipole correction) and to 18 K from 24 K (without the dipole correction). Only in the case with the dipole correction, T_c approaches the experimental value. This will remain robust (or even be reinforced) by taking account of the general tendency of the mean field theory to overestimate T_c (assuming that the tunneling correction will not be larger than Ω).

4 Concluding Remarks

In summary, we have investigated the properties of the hydrogen-bonded antiferroelectrics, BrHPLN, by means of the electronic structure calculations and Monte Carlo methods. The significant charge density which amounts to 0.01 e bohr^{-3} has been found in the intermolecular region. This suggests that BrHPLN has the one-dimensional intermolecular chains of the $C-H\cdots O$ type weak hydrogen bonds shown in Fig. 6, and these bonds increase covalency. The MC method with the correction of the molecular dipole moment has been proposed to evaluate the dielectric properties including the effect of the intermolecular hydrogen bonding. Our calculation results show

that a phase transition occurs from a paraelectric phase to an antiferroelectric phase at 50 K. This transition temperature is the same order as the experimental results. In present work, we have treated BrHPLN only. However, the above discussion on the intermolecular hydrogen bonding is applicable to MeH-PLN and IHPLN, because of their similarity in the molecular and crystal structure. We will apply our method to other materials and extend our method to the quantum Monte Carlo method in the future.

Acknowledgments

References

1 J. Valasek, *Phys. Rev.*, 1920, **15**, 537.

2 J. Valasek, *Phys. Rev.*, 1921, **17**, 475.

3 S. Horiuchi and Y. Tokura, *Nat. Mater.*, 2008, **7**, 357.

4 T. Akutagawa, H. Koshinaka, D. Sato, S. Takeda, S.-I. Noro, H. Takahashi, R. Kumai, Y. Tokura and T. Nakamura, *Nat. Mater.*, 2009, **8**, 342.

5 G. Busch and P. Scherrer, *Naturwiss.*, 1935, **23**, 737.

6 K. Gesi, *J. Phys. Soc. Jpn.*, 1980, **48**, 886.

7 D. Semmingsen and J. Feder, *Solid State Commun.*, 1974, **15**, 1369.

8 F. Jona and G. Shirane, *Ferroelectric Crystals*, Pergamon Press, 1962.

9 W. C. Hamilton and J. A. Ibers, *Hydrogen Bonding in Solids: Methods of Molecular Structure Determination*, W. A. Benjamin, Inc., New York, 1968.

10 R. Blinc and B. Žekš, *Adv. Phys.*, 1972, **21**, 693.

11 Y. Moritomo, Y. Tokura, N. Nagaosa, T. Suzuki and K. Kumagai, *Phys. Rev. Lett.*, 1993, **71**, 2833.

12 T. Mochida, A. Izuoka, T. Sugawara, Y. Moritomo and Y. Tokura, *J. Chem. Phys.*, 1994, **101**, 7971.

13 H. Sugimoto, *J. Phys.: Condens. Matter*, 1998, **10**, 1237.

14 Y. Moritomo, Y. Tokura, T. Mochida, A. Izuoka and T. Sugawara, *J. Phys. Soc. Jpn.*, 1995, **64**, 1892.

15 Y. Noda, T. Hayashide, I. Tamura, T. Mochida and T. Sugawara, *J. Korean Phys. Soc.*, 1998, **32**, S8.

16 T. Matsuo, K. Kohno, A. Inaba, T. Mochida, A. Izuoka and T. Sugawara, *J. Chem. Phys.*, 1998, **108**, 9809.

17 T. Matsuo, K. Kohno, M. Ohama, T. Mochida, A. Izuoka and T. Sugawara, *Europhys. Lett.*, 1999, **47**, 36.

18 I. Tamura, Y. Noda, Y. Kuroiwa, T. Mochida and T. Sugawara, *J. Phys.: Condens. Matter*, 2000, **12**, 8345.

19 T. Matsuo, S. Baluja, Y. Koike, M. Ohama, T. Mochida and T. Sugawara, *Chem. Phys. Lett.*, 2001, **342**, 22.

20 T. Matsuo, M. Ohama, T. Mochida and T. Sugawara, *J. Mol. Struct.*, 2004, **700**, 127.

21 T. Matsuo, O. Yamamuro, A. Inaba, M. Ohama, T. Mochida and T. Sugawara, *Ferroelectrics*, 2007, **347**, 101.

22 R. Kiyanagi, A. Kojima, T. Hayashide, H. Kimura, M. Watanabe, Y. Noda, T. Mochida, T. Sugawara and S. Kumazawa, *J. Phys. Soc. Jpn.*, 2003, **72**, 2816.

23 Y. Noda, R. Kiyanagi, H. Kimura, M. Watanabe, A. Kojima, T. Hayashide, T. Mochida and T. Sugawara, *Ferroelectrics*, 2002, **269**, 327.

24 R. Kiyanagi, H. Kimura, M. Watanabe, Y. Noda, A. Kojima, T. Hayashide, T. Mochida, T. Sugawara and S. Kumazawa, *J. Korean Phys. Soc.*, 2003, **42**, S1279.

25 R. Kiyanagi, A. Kojima, H. Kimura, M. Watanabe, Y. Noda, T. Mochida and T. Sugawara, *J. Phys. Soc. Jpn.*, 2005, **74**, 613.

26 R. Kiyanagi, H. Kimura, M. Watanabe, Y. Noda, T. Mochida and T. Sugawara, *J. Korean Phys. Soc.*, 2005, **46**, 239.

27 R. Kiyanagi, H. Kimura, M. Watanabe, Y. Noda, T. Mochida and T. Sugawara, *J. Phys. Soc. Jpn.*, 2008, **77**, 064602.

28 Y. Noda, I. Tamura, Y. Kuroiwa, T. Mochida and T. Sugawara, *J. Phys. Soc. Jpn.*, 1994, **63**, 4286.

29 K. Momma and F. Izumi, *J. Appl. Crystallogr.*, 2008, **41**, 653.

30 C. Totsuji and T. Matsubara, *J. Phys. Soc. Jpn.*, 1994, **63**, 2760.

31 C. Totsuji, *J. Phys. Soc. Jpn.*, 2004, **73**, 1054.

32 S. P. Dolin, A. A. Khrulev, E. V. Polyakov, T. Y. Mikhailova and A. A. Levin, *Int. J. Quantum Chem.*, 2006, **106**, 2297.

33 S. P. Dolin, A. A. Levin, E. V. Polyakov, A. A. Khrulev and T. Y. Mikhailova, *J. Mol. Struct.*, 2006, **790**, 147.

34 B. K. Chakrabarti, A. Dutta and P. Sen, *Quantum Ising Phases and Transitions in Transverse Ising Models*, Springer-Verlag, Berlin, 1996.

35 S. Horiuchi, F. Ishii, R. Kumai, Y. Okimoto, H. Tachibana, N. Nagaosa and Y. Tokura, *Nat. Mater.*, 2005, **4**, 163.

36 F. Ishii, N. Nagaosa, Y. Tokura and K. Terakura, *Phys. Rev. B*, 2006, **73**, 212105.

37 G. A. Jeffrey and W. Saenger, *Hydrogen Bonding in Biological Structures*, Springer-Verlag, Berlin, 1991.

38 G. R. Desiraju and T. Steiner, *The Weak Hydrogen Bond*, Oxford University Press, New York, 2001.

39 J. Kohanoff, *Electronic Structure Calculations for Solids and Molecules: Theory and Computational Methods*, Cambridge University Press, Cambridge, 2006.

40 K. Kitaura, E. Ikeo, T. Asada, T. Nakano and M. Uebayasi, *Chem. Phys. Lett.*, 1999, **313**, 701.

41 R. D. King-Smith and D. Vanderbilt, *Phys. Rev. B*, 1993, **47**, 1651.

42 R. Resta, *Rev. Mod. Phys.*, 1994, **66**, 899.

43 P. Giannozzi, S. Baroni, N. Bonini, M. Calandra, R. Car, C. Cavazzoni, D. Ceresoli, G. L. Chiarotti, M. Cococcioni, I. Dabo, A. Dal Corso, S. de Gironcoli, S. Fabris, G. Fratesi, R. Gebauer, U. Gerstmann, C. Gougoussis, A. Kokalj, M. Lazzeri, L. Martin-Samos, N. Marzari, F. Mauri, R. Mazzarello, S. Paolini, A. Pasquarello, L. Paulatto, C. Sbraccia, S. Scandolo, G. Sclauzero, A. P. Seitsonen, A. Smogunov, P. Umari and R. M. Wentzcovitch, *J. Phys.: Condens. Matter*, 2009, **21**, 395502.

44 M. W. Schmidt, K. K. Baldridge, J. A. Boatz, S. T. Elbert, M. S. Gordon, J. H. Jensen, S. Koseki, N. Matsunaga, K. A. Nguyen, S. Su, T. L. Windus, M. Dupuis and J. A. Montgomery, *J. Comput. Chem.*, 1993, **14**, 1347.

45 K. Hukushima and K. Nemoto, *J. Phys. Soc. Jpn.*, 1996, **65**, 1604.

46 A. E. Reed, L. A. Curtiss and F. Weinhold, *Chem. Rev.*, 1988, **88**, 899.

47 K. Binder and D. W. Heermann, *Monte Carlo Simulation in Statistical Physics: An Introduction*, Springer, 5th edn, 2010.

48 P. G. de Gennes, *Solid State Commun.*, 1963, **1**, 132.

49 M. E. Lines and A. M. Glass, *Principles and Applications of Ferroelectrics and Related Materials*, Oxford University Press, 1977.

50 V. E. Bondybey, R. C. Haddon and J. H. English, *J. Chem. Phys.*, 1984, **80**, 5432.

51 Y. Moritomo, Y. Tokura, N. Nagaosa, T. Suzuki and K. Kumagai, *J. Low Temp. Phys.*, 1995, **99**, 55.

Supplementary Material for

The Role of Intermolecular Hydrogen Bond

on Dielectric Properties in Hydrogen-Bonded Material

5-Bromo-9-hydroxyphenalenone: Theoretical Investigation

Hiroki Otaki[*] and Koji Ando

Department of Chemistry, Graduate School of Science,

Kyoto University, Sakyo-ku, Kyoto 606-8502, Japan
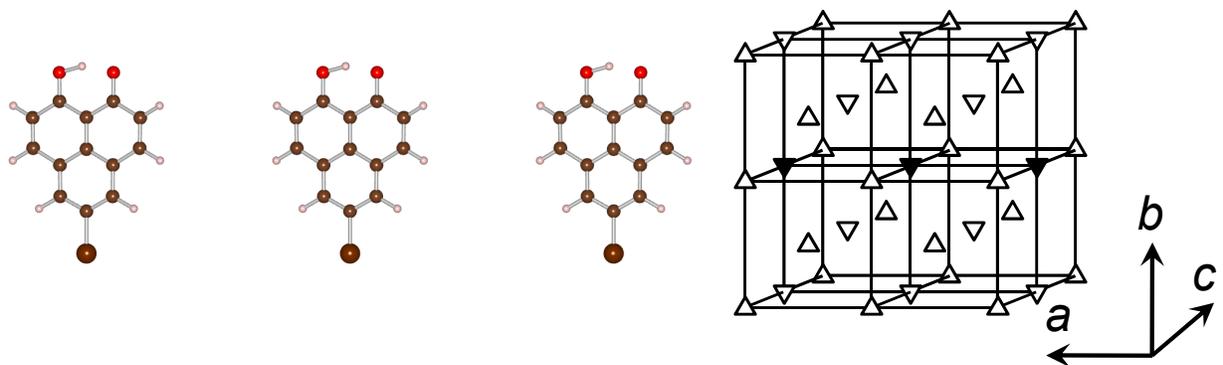
FIG. S1. Schematic structure of trimer A and its position in the crystal. Each triangle indicates a BrH-PLN molecule and inverted triangle represents an inverted one. The three solid triangles correspond to the components of the trimer.
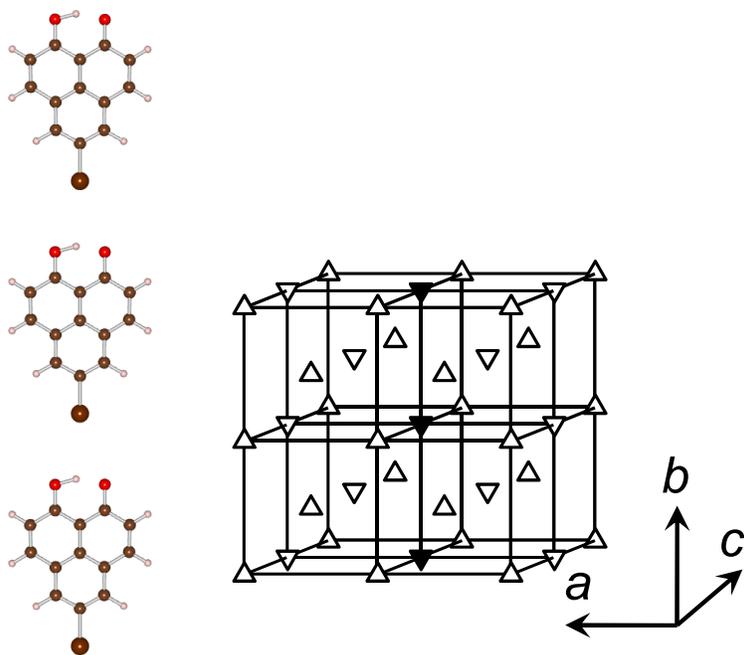

FIG. S2. Same as Fig. S1, but for trimer B.
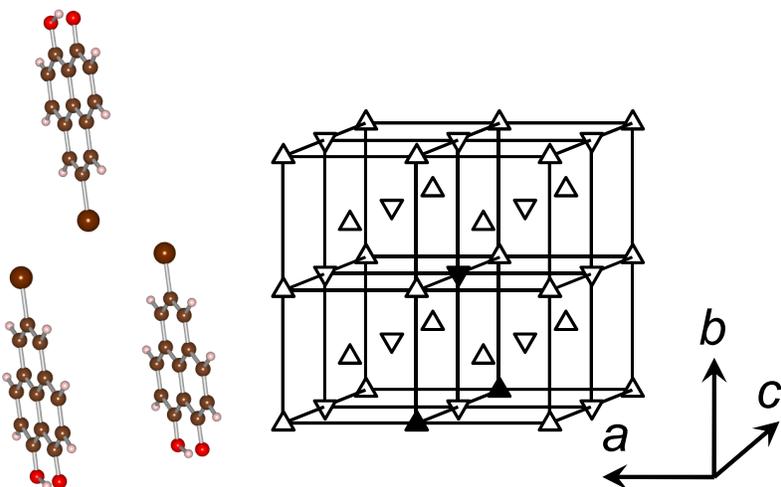
FIG. S3. Same as Fig. S1, but for trimer C.
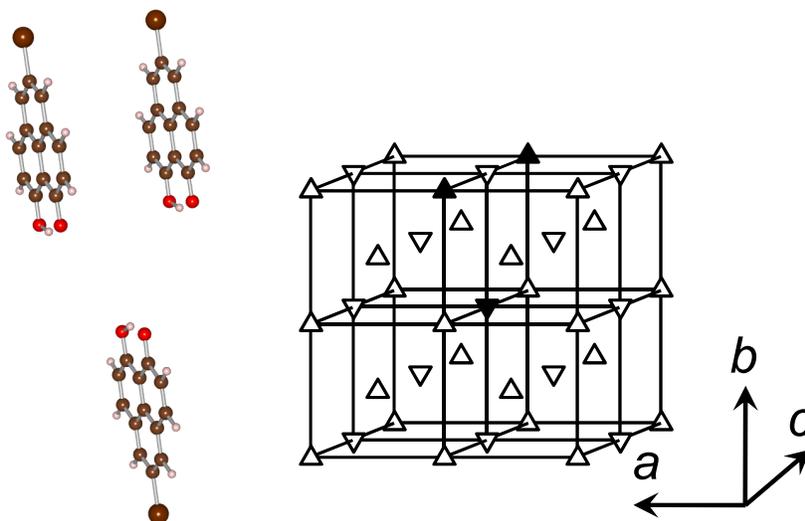
FIG. S4. Same as Fig. S1, but for trimer D.
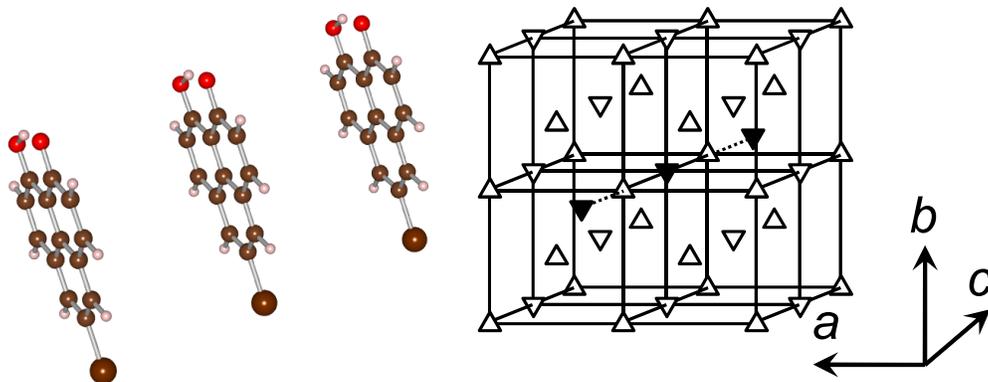
FIG. S5. Same as Fig. S1, but for trimer E.
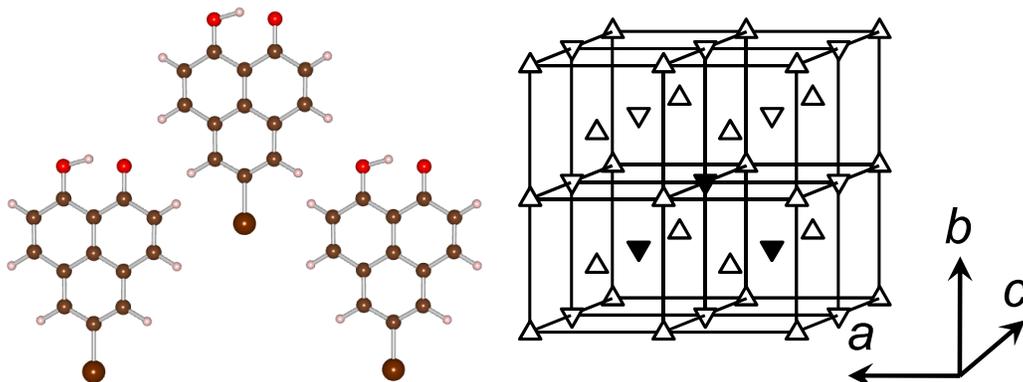
FIG. S6. Same as Fig. S1, but for trimer F.
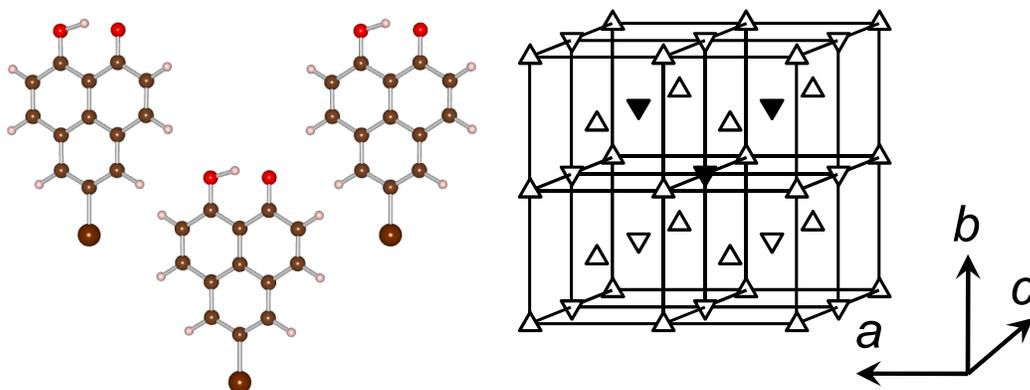
FIG. S7. Same as Fig. S1, but for trimer G.
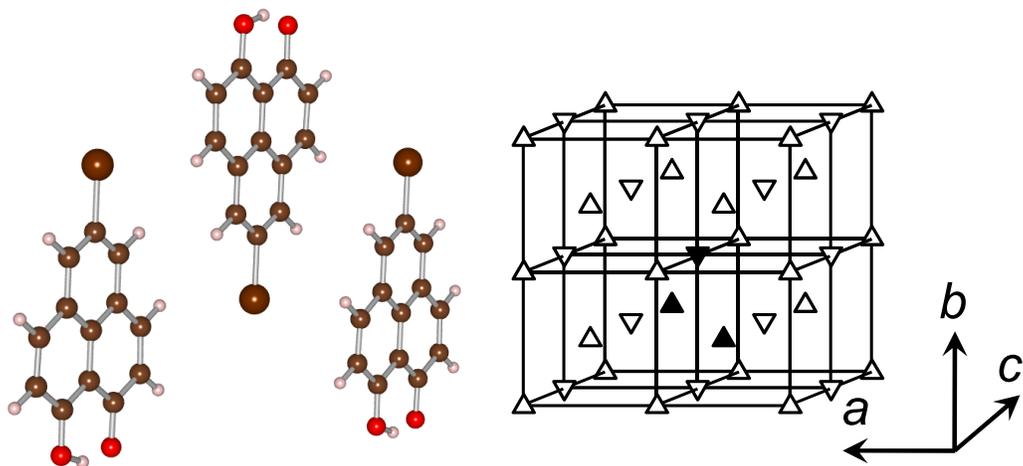
FIG. S8. Same as Fig. S1, but for trimer H.
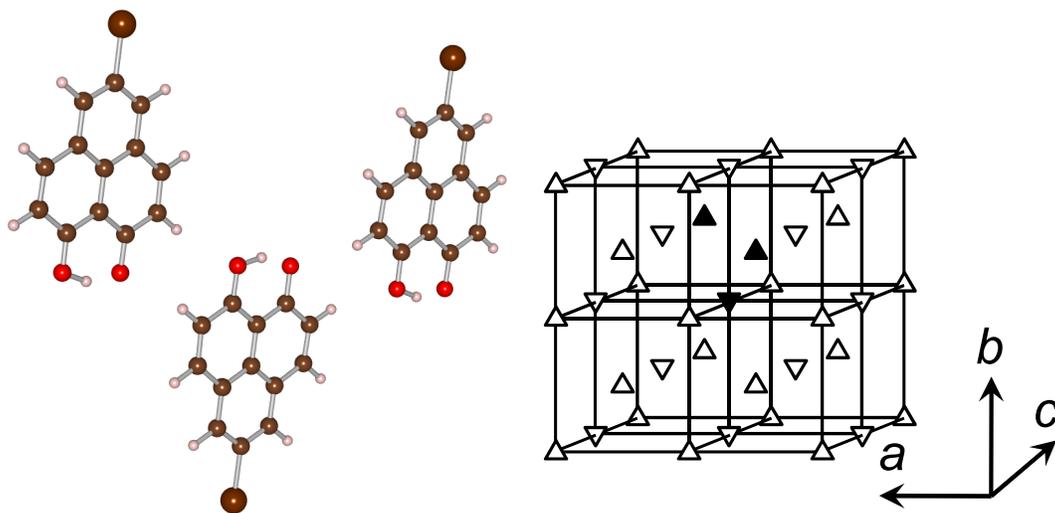
FIG. S9. Same as Fig. S1, but for trimer I.
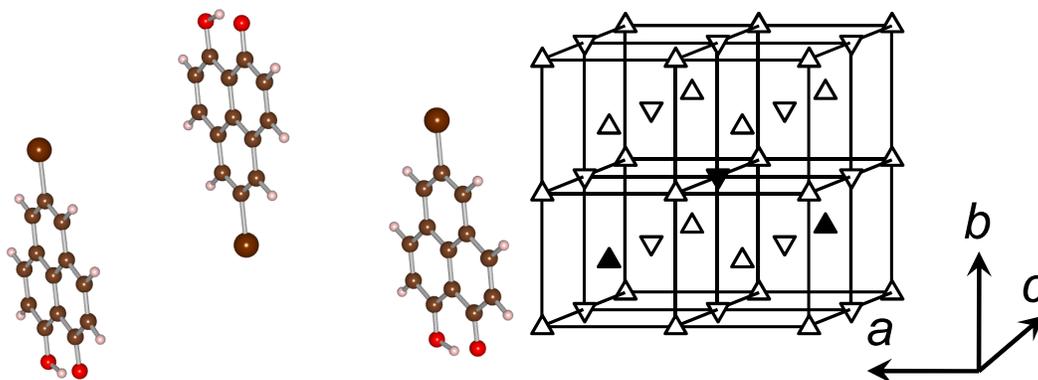
FIG. S10. Same as Fig. S1, but for trimer J.
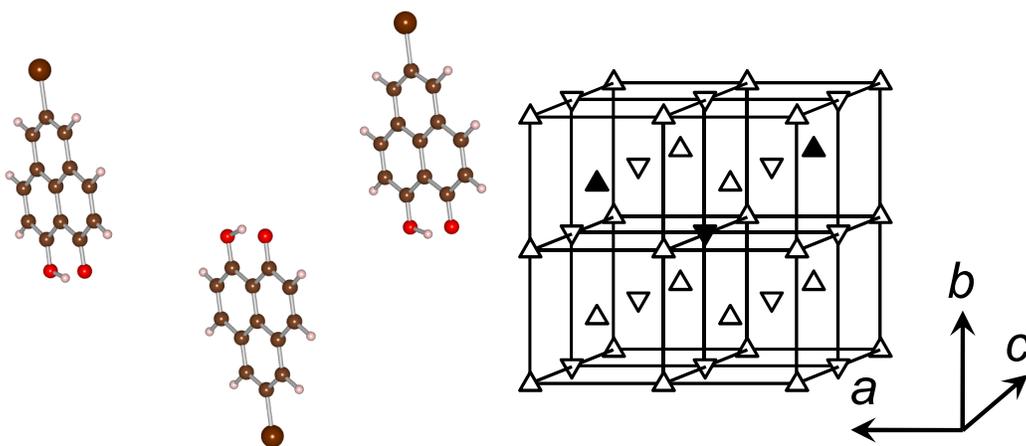
FIG. S11. Same as Fig. S1, but for trimer K.
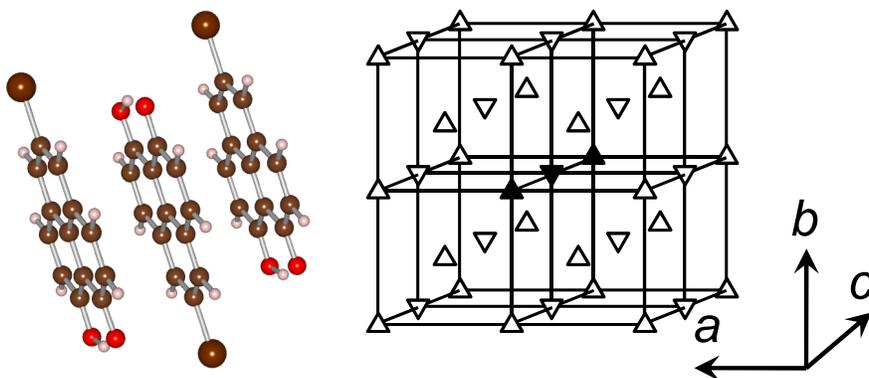
FIG. S12. Same as Fig. S1, but for trimer L.
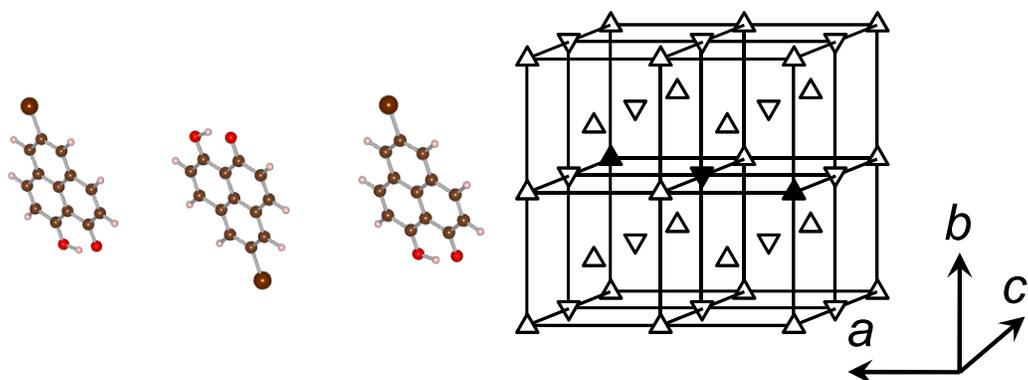
FIG. S13. Same as Fig. S1, but for trimer M.
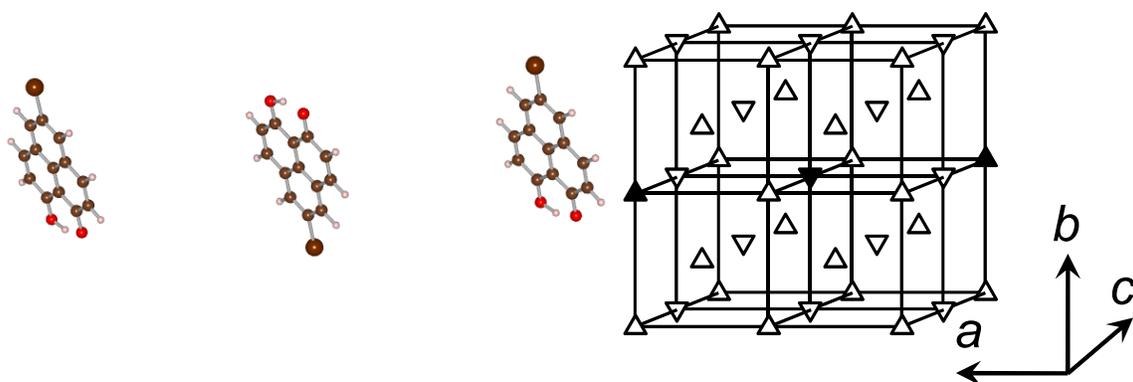
FIG. S14. Same as Fig. S1, but for trimer N.
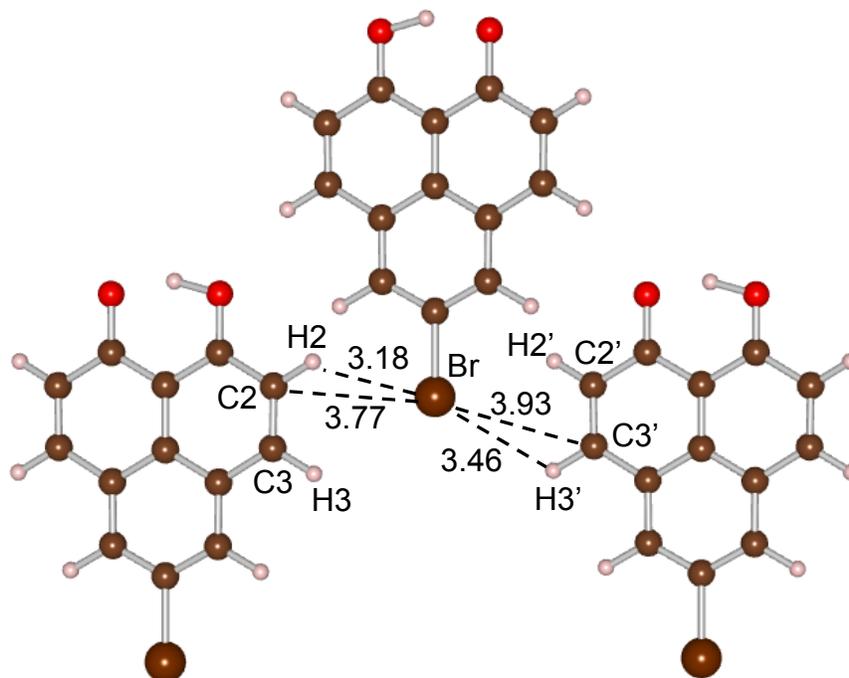
FIG. S15. Schematic structure of trimer F. The values in the figure denote the distances between atoms (in Å). Labels for atoms are given for Table S1.

TABLE S1. NPA charges for an isolated monomer and the central molecule of trimer F. The charges of the atoms around the Br atom of the central molecule are shown

	HF/3-21G(d,p)		HF/6-31G(d,p)	
Atom	Isolated	Central	Isolated	Central
Br	0.078	0.056	0.062	0.037
H2$'$	0.249	0.251	0.254	0.255
C2$'$	−0.323	−0.334	−0.317	−0.330
H3$'$	0.236	0.239	0.242	0.246
C3$'$	−0.109	−0.099	−0.112	−0.100
H2	0.249	0.253	0.254	0.256
C2	−0.334	−0.342	−0.327	−0.336
H3	0.238	0.241	0.244	0.249
C3	−0.095	−0.087	−0.099	−0.090